

## Supplementary Information

### Ultrafast Rechargeable Zn Micro-Batteries Endowing Wearable Solar Charging System with High Overall Efficiency

Zhengnan Tian,<sup>1,2†</sup> Zhongti Sun,<sup>1,2†</sup> Yanyan Shao,<sup>1,2</sup> Liang Gao,<sup>1</sup> Rong Huang,<sup>1</sup> Yuanlong Shao,<sup>1,2,3\*</sup>  
Richard B. Kaner,<sup>4\*</sup> and Jingyu Sun<sup>1,2,3\*</sup>

<sup>1</sup>*College of Energy, Soochow Institute for Energy and Materials Innovations (SIEMIS), Jiangsu Provincial Key Laboratory for Advanced Carbon Materials and Wearable Energy Technologies, Soochow University, Suzhou 215006, P. R. China.*

<sup>2</sup>*SUDA-BGI Collaborative Innovation Center, Soochow University, Suzhou 215006, P. R. China.*

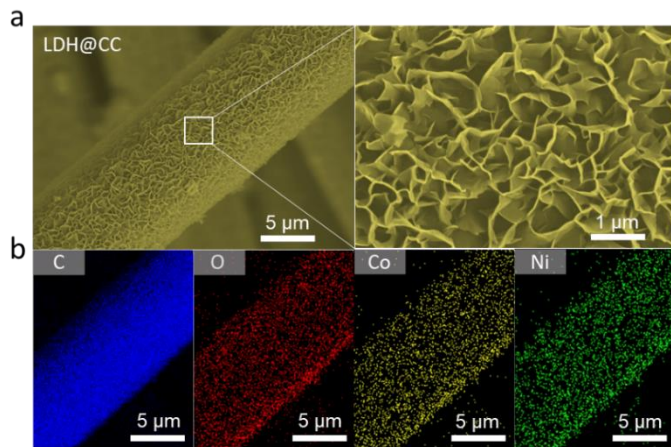
<sup>3</sup>*Beijing Graphene Institute (BGI), Beijing 100095, P. R. China.*

<sup>4</sup>*Department of Chemistry and Biochemistry, Department of Materials Science and Engineering, and California NanoSystems Institute, University of California, Los Angeles (UCLA), USA.*

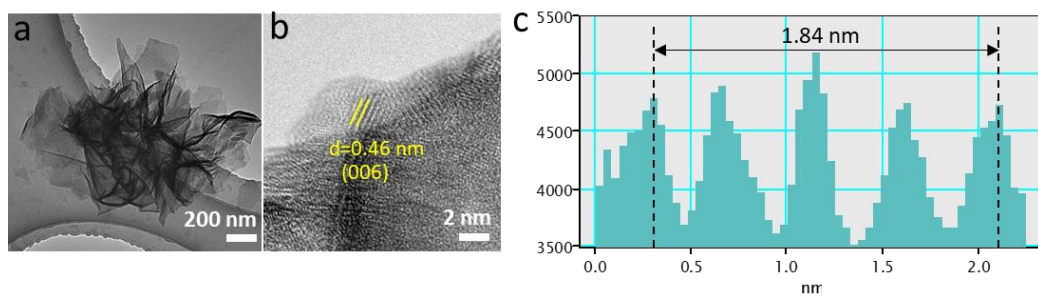
\*Corresponding authors. E-mail: sunjy86@suda.edu.cn (J.S.); ylshao@suda.edu.cn (Y.S.); kaner@chem.ucla.edu (R.B.K.)

†These authors contributed equally to this work.

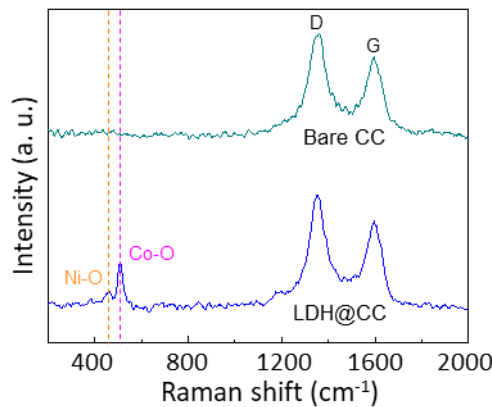
## Supplementary Figures



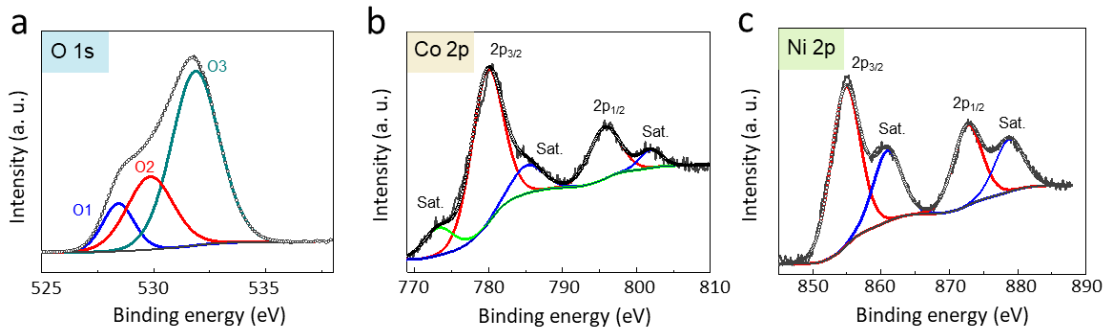
**Supplementary Figure 1. SEM characterization of LDH@CC.** (a) SEM images of LDH@CC. (b) Elemental mapping of C, O, Co and Ni in the as-synthesized LDH@CC material.



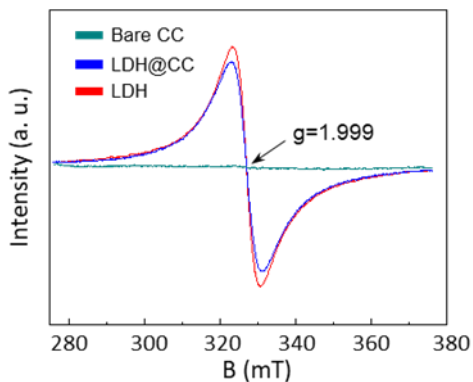
**Supplementary Figure 2. TEM characterization of LDH@CC.** (a) TEM image of LDH nanosheets. (b) High-resolution TEM image. (c) The lattice spacing corresponding to the (006) plane.



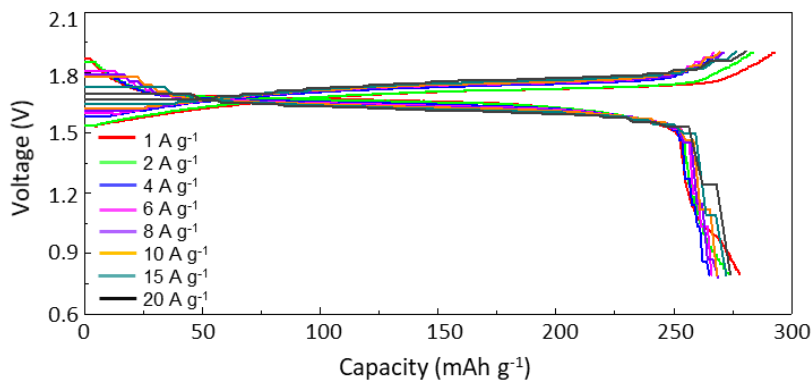
**Supplementary Figure 3. Raman spectra of bare CC and LDH@CC.** ‘Bare CC’ represents the original carbon cloth experiencing the same hydrothermal process without the addition of metal salts.



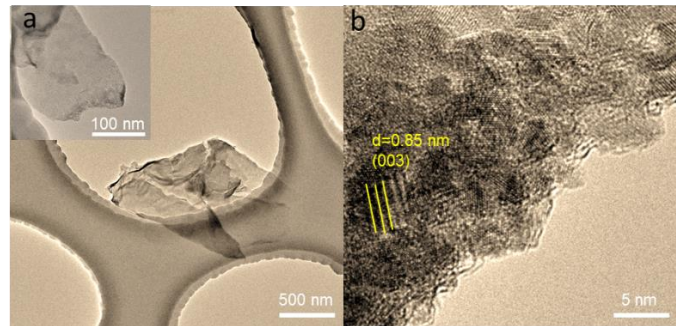
**Supplementary Figure 4. XPS spectra of the LDH@CC material.** (a) O 1s. (b) Co 2p. (c) Ni 2p. (O1: oxygen atoms bound to metals; O2: surface oxygen defect species; O3: hydroxyl groups or surface-adsorbed oxygen)



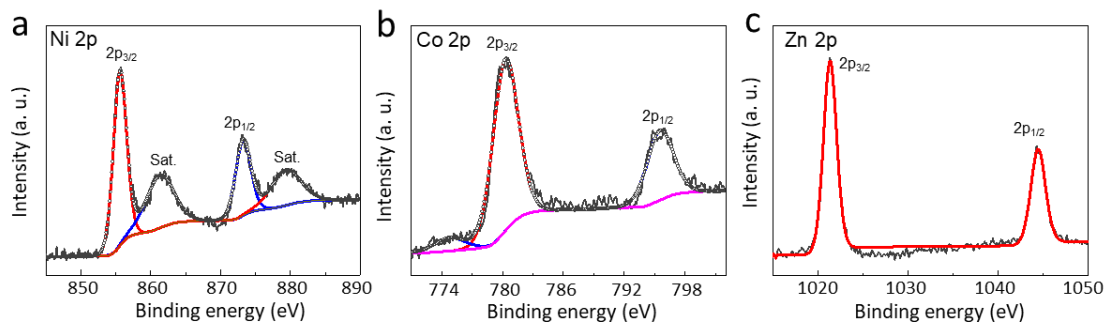
**Supplementary Figure 5. ESR spectra of bare CC, LDH@CC and LDH material.**



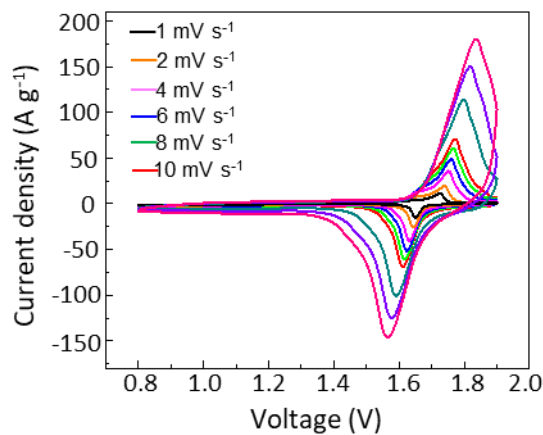
**Supplementary Figure 6. GCD curves of the ZIB under different current densities from 1 to 20 A g<sup>-1</sup>.**



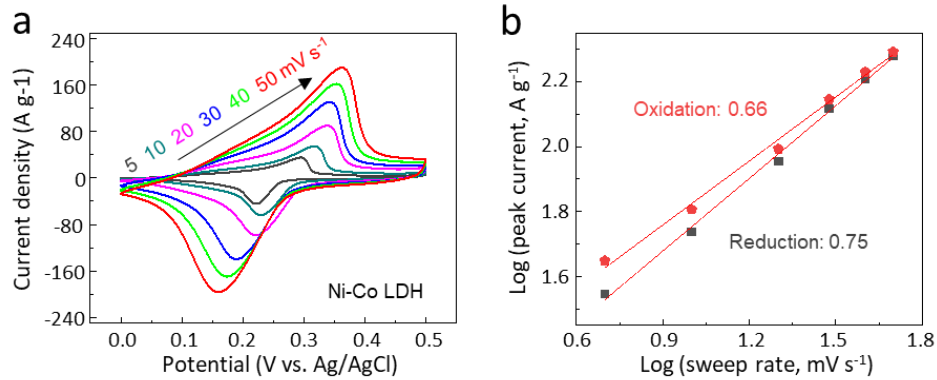
**Supplementary Figure 7. TEM images of the LDH@CC material after 1000 cycles.** (a) The nanosheet morphology at low magnification. (b) The lattice spacing corresponding to the (003) plane.



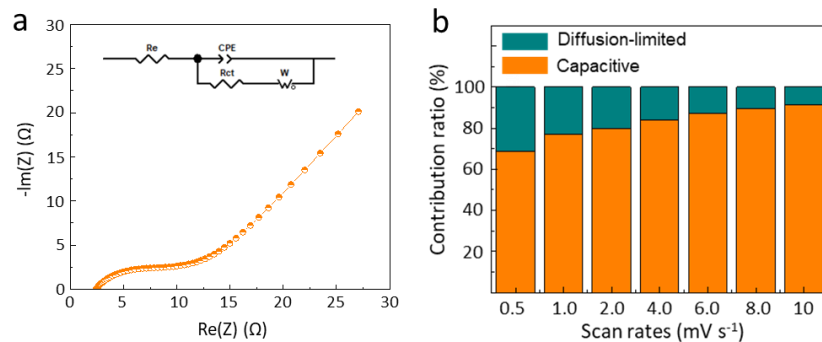
**Supplementary Figure 8. XPS spectra of the LDH@CC material after 1000 cycles.** (a) Ni 2p. (b) Co 2p. (c) Zn 2p.



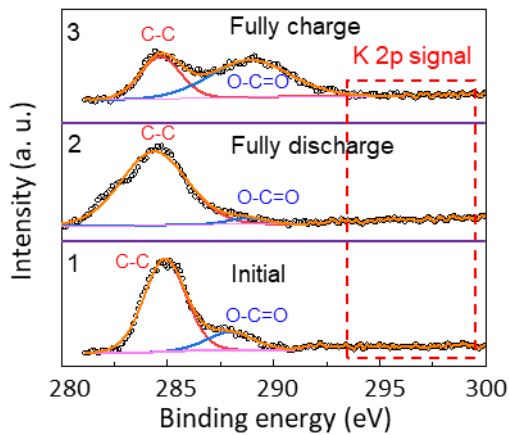
**Supplementary Figure 9. CV curves of the assembled ZIB at different scan rates from 1 to 10 mV s<sup>-1</sup>.**



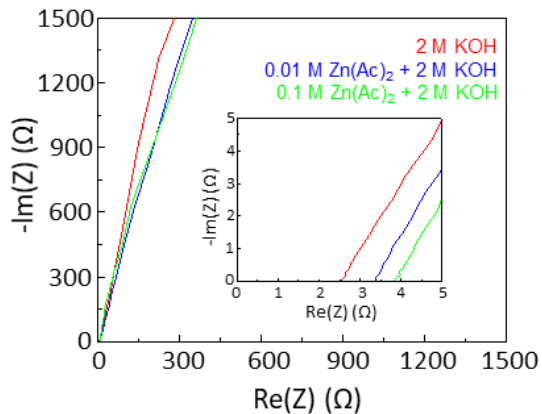
**Supplementary Figure 10.** Three-electrode evaluation of the LDH@CC. (a) CV curves at different scan rates from 5 to 50  $\text{mV s}^{-1}$ . (b)  $b$ -value calculation according to the CV curves (employed electrolyte: 2.0 M KOH + 0.01 M  $\text{Zn}(\text{CH}_3\text{COO})_2$ ).



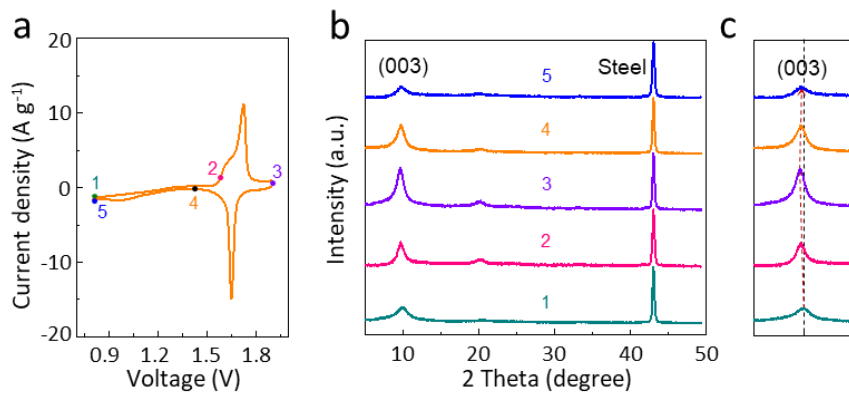
**Supplementary Figure 11.** (a) Nyquist plot of the ZIB. (b) The capacitive and diffusion-limited contribution calculated according to the CV curves.



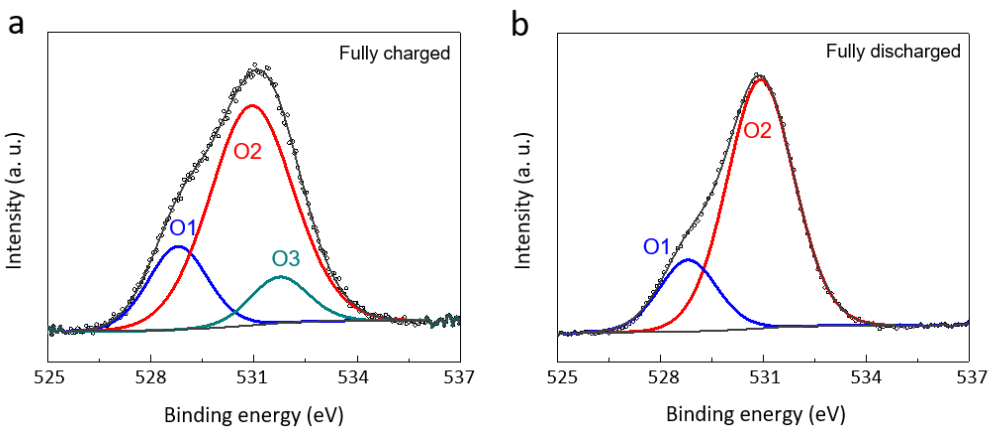
**Supplementary Figure 12.** *Ex situ* K 2p XPS spectra of the LDH@CC.



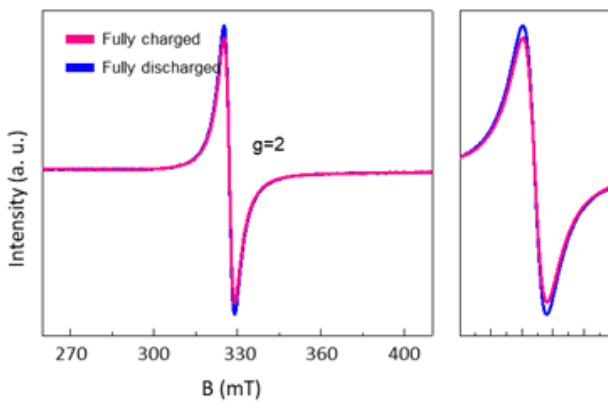
**Supplementary Figure 13.** Nyquist plots in three different electrolytes (red color: 2 M KOH; blue color: 2 M KOH + 0.01 M  $\text{ZnAc}_2$ ; green color: 2 M KOH + 0.1 M  $\text{ZnAc}_2$ ). The bare carbon cloth was employed as the working electrode where the zinc plate was used as the counter electrode.



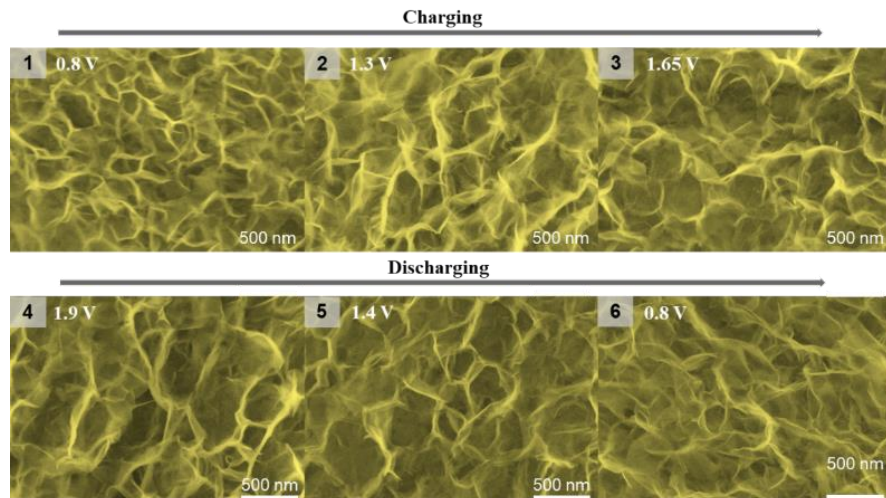
**Supplementary Figure 14.** *Ex situ* high-resolution XRD measurements of the LDH material pasted onto the stainless-steel foil (employed electrolyte: 2.0 M KOH + 0.01 M  $\text{ZnAc}_2$ ).



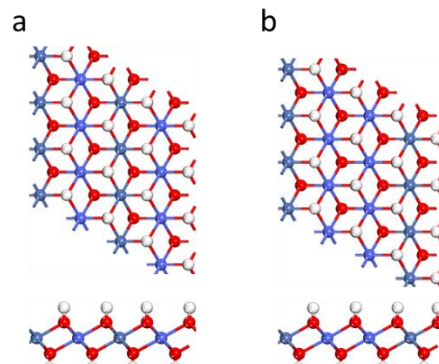
**Supplementary Figure 15. High-resolution O 1s XPS spectra at (a) fully charged and (b) fully discharged states.** O1 represents the oxygen atom bound to metals, O2 reflects the contribution from the oxygen vacancy sites and O3 indicates the existence of hydroxyl groups or surface-adsorbed oxygen. There are two obvious differences between the fully charged and fully discharged electrodes: (i) The increase of O2 contribution (from 60% to 85%), which illustrates the increase of oxygen vacancy. The O2 increase is related to the augmentation of oxygen defects according to the deintercalation of hydroxyl ions from the surface of LDH@CC electrode. (ii) The vanish of O3 contribution. O3 mainly denotes the surface adsorbed hydroxyl groups. From fully charge to fully discharge state, the hydroxyl group would dissociate from the surface of LDH material, which is also related to the deintercalation process of hydroxide ions.



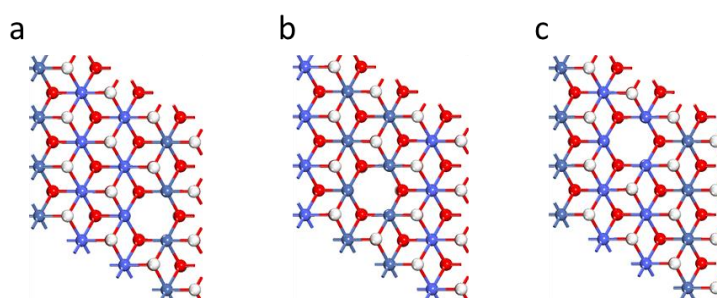
**Supplementary Figure 16. Ex situ ESR spectra of LDH@CC at different states (red line: fully charged state; blue line: fully discharged state).**



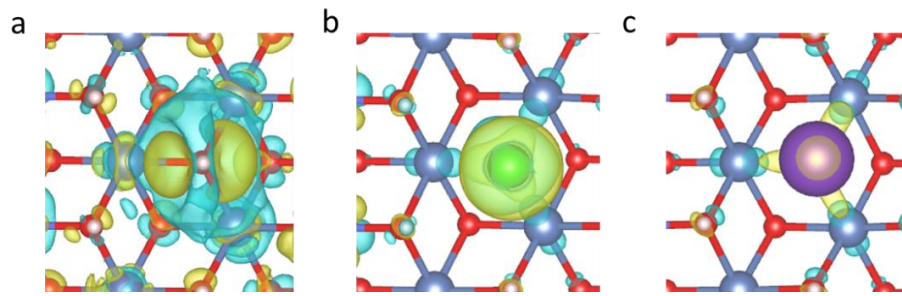
**Supplementary Figure 17.** *Ex situ* SEM images of the LDH@CC.



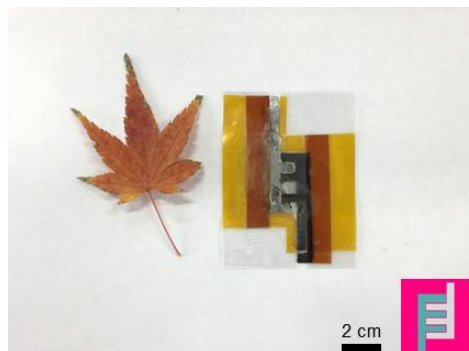
**Supplementary Figure 18.** The top (up) and side (down) views of two possible configurations of the LDH monolayer. A lower energy state shown in (b) as compared to (a) by 0.04 eV for the 4×4 supercell (steel-blue, blue, red, and white ball denotes as Ni, Co, O, and H atom, respectively).



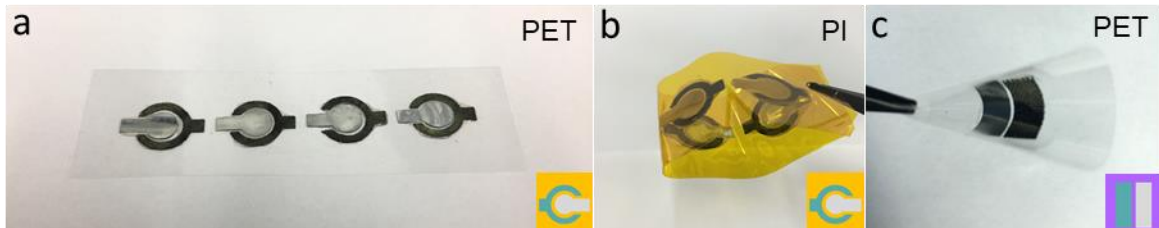
**Supplementary Figure 19.** Three possible configurations of LDH monolayer with O vacancy (VO), named as VO-NiCo (a), VO-Ni (b), and VO-Co (c). (b) possesses the lowest energy than (a) and (c) by 0.03 eV and 0.09 eV, respectively (steel-blue, blue, red, and white ball denotes as Ni, Co, O, and H atom, respectively).



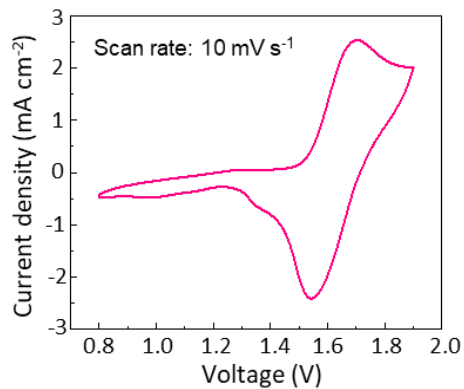
**Supplementary Figure 20. Difference charge density diagram adsorption configuration.** (a) OH. (b) Zn. (c) K. Yellow and cyan contour with the isosurface value of  $0.0013 \text{ \AA}/\text{Bohr}^3$  indicates augmented and reduced charge density, respectively (steel-blue, blue, red, white, green, and violet ball represents Ni, Co, O, H, Zn, and K atoms, respectively).



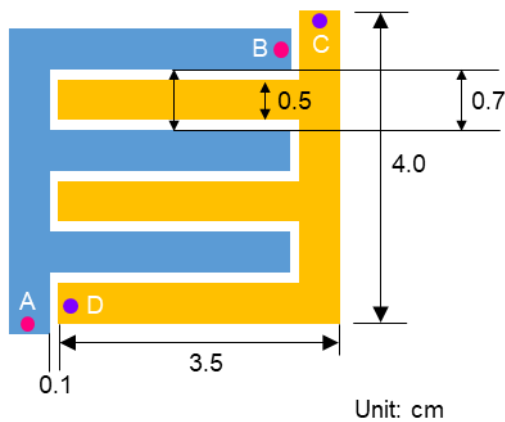
**Supplementary Figure 21. Digital photo of an interdigitated micro-ZIB.**



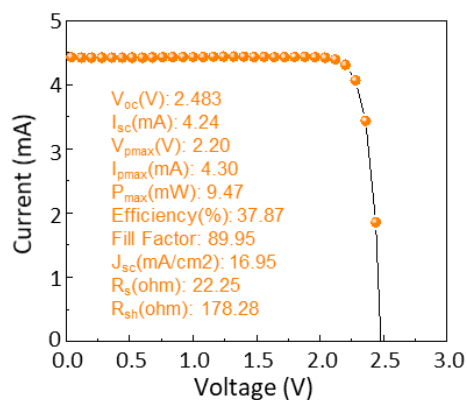
**Supplementary Figure 22. Digital photos of micro-ZIBs on different substrates.** (a) Concentric structure on a flexible PET substrate. (b) Concentric structure on a flexible PI substrate. (c) Strip structure on a flexible PET substrate.



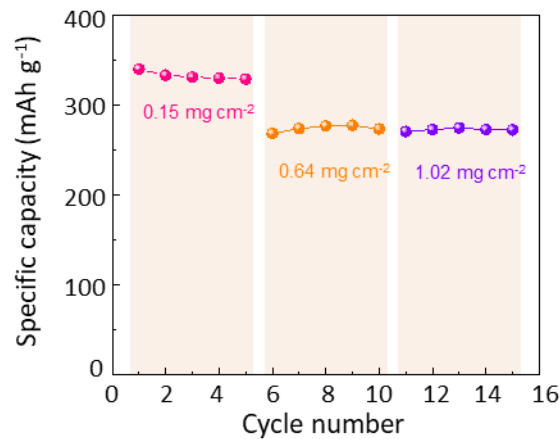
**Supplementary Figure 23.** CV curve of the micro-ZIB device at a scan rate of  $10 \text{ mV s}^{-1}$ .



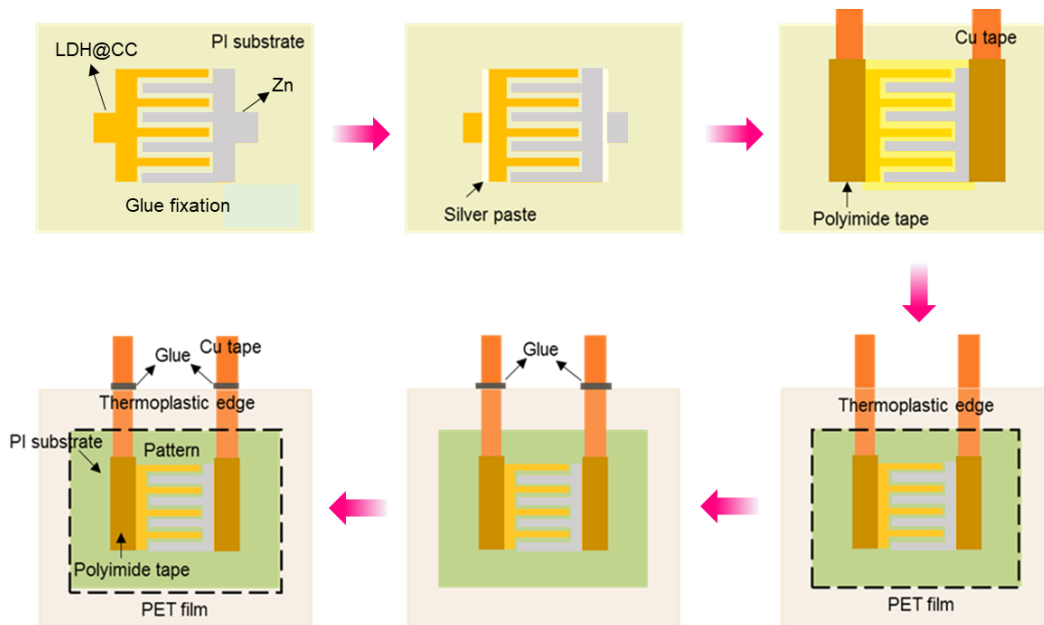
**Supplementary Figure 24.** Detailed dimensions of the interdigital finger-like micro-ZIB. A and B represent the two furthest points of the LDH@CC cathode; C and D represent the two furthest points of the Zn plate anode.



**Supplementary Figure 25.** J-V curve of the GaAs solar cell.



**Supplementary Figure 26.** Specific capacity values of ZIBs in coin-cell configuration with different LDH mass loadings ( $0.15$ ,  $0.64$  and  $1.02\text{ mg cm}^{-2}$ ).



**Supplementary Figure 27.** The encapsulation process of the micro-ZIB.

## Supplementary Tables

**Supplementary Table 1. Performance comparison of related zinc-based battery systems.**

Cathode Material	Electrolyte	Maximum Energy Density (Wh Kg <sup>-1</sup> )	Maximum Power Density (W Kg <sup>-1</sup> )	Rate Performance (%)	Capacity Retention (%)	Ref.
Ni-Co LDH	KOH	445	30885.71	97.17	98.6 (1 to 20 A g <sup>-1</sup> )	This work
Zn <sub>0.3</sub> V <sub>2</sub> O <sub>5</sub>	Zn(CF <sub>3</sub> SO <sub>3</sub> ) <sub>2</sub>	336	6000	50.60	68.2 (1 to 10 A g <sup>-1</sup> )	1
P-NiCo <sub>2</sub> O <sub>4-x</sub>	KOH	616.5	30000	61.64	60.4 (6 to 60 A g <sup>-1</sup> )	2
NaV <sub>3</sub> O <sub>8</sub> ·1.5H <sub>2</sub> O	ZnSO <sub>4</sub>	300	3600	50.00	44 (0.1 to 4 A g <sup>-1</sup> )	3
V <sub>2</sub> O <sub>5</sub> ·nH <sub>2</sub> O	Zn(CF <sub>3</sub> SO <sub>3</sub> ) <sub>2</sub>	290	12200	58.97	67 (0.3 to 30 A g <sup>-1</sup> )	4
NiO	KOH	355.7	17900	53.42	58 (0.5 to 20 mA cm <sup>-2</sup> )	5
NiAlCo-LDH	KOH	324	40000	69.44	76.4 (3 to 65 A g <sup>-1</sup> )	6
Co@Ni(OH) <sub>2</sub>	KOH	148.5	138000	77.42	55 (5 to 15 A g <sup>-1</sup> )	7
NiCo <sub>2</sub> O <sub>4</sub>	KOH	290	49000	54.97	61.4 (1.6 to 19 A g <sup>-1</sup> )	8

Annotation: Rate performance represents the ratio of the highest energy density to the energy density achieving at the highest power density.

**Supplementary Table 2. Equivalent circuit parameter fitting from the plot in Supplementary Fig. 11.**

R <sub>e</sub>	CPE-T	CPE-P	R <sub>ct</sub>	W-R	W-T	W-P
2.393	0.004	0.671	5.439	15.08	6.746	0.297

**Supplementary Table 3. Performance comparison of recently reported in-plane energy storage devices.**

Cathode//Anode	Electrolyte	Energy Density (μWh cm <sup>-2</sup> )	Voltage Window (V)	Flexibility (bending cycles)	Ref.
Ni-Co LDH//Zn	KOH	135.61	0.8-1.9	1000	This work
AC//Zn	ZnSO <sub>4</sub>	115.40	0.5-1.5	N/A	9
MnO <sub>2</sub> //VN	MgSO <sub>4</sub>	19.13	0.0-2.2	N/A	10
NiCoP//ZIF-C	KOH	13.90	0.0-1.4	500	11
Cu(OH) <sub>2</sub> @FeOOH	[EMIM][BF <sub>4</sub> ]	18.07	0.0-1.5	1000	12
MoS <sub>2</sub> @CNT	KOH	148.50	0.0-1.0	N/A	13
MnO <sub>2</sub> @PPY	KOH	290.00	0.0-1.6	N/A	14
MXene	H <sub>2</sub> SO <sub>4</sub>	0.32	0.0-0.5	1000	15
MnO <sub>2</sub> /Ppy	Na <sub>2</sub> SO <sub>4</sub>	8.05	0.0-1.5	N/A	16
Ni-CAT//LSG	LiCl	4.10	0.0-1.4	N/A	17

**Supplementary Table 4. The related parameters of the constructed wearable solar charging systems.**

Energy Conversion System	Energy Storage System	Overall Efficiency (%)	Solar Charging Time (h)	Cycle Performance	Ref.
GaAs	ZIB	23.11	5	100	This work
GaAs	ASC	17.57	3	100	10
GaAs	FB	14.10	1800	10	18
DSSC	ZIB	N/A	60	N/A	19
PSC	SSC	10.00	N/A	N/A	20
PSC	LIB	9.36	3600	10	21
PSC	LIC	8.41	1800	7	22
PSC	LIB	7.80	7200	15	23
DSSC	LIB	5.50	9000	10	21
PSC	SSC	5.10	125	1000	24
OSC	SSC	2.92	N/A	N/A	25

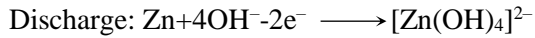
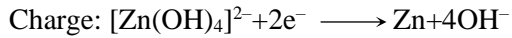
Annotation: PSC: perovskite solar cell; DSSC: dye sensitized solar cell; OSC: organic solar battery; ASC: asymmetric supercapacitor; SSC: symmetric supercapacitor; ZIB: zinc-ion battery; FB: flow battery; LIB: lithium-ion battery; LIC: lithium-ion capacitor.

## Supplementary Notes

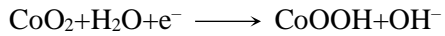
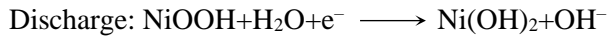
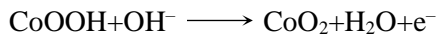
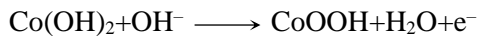
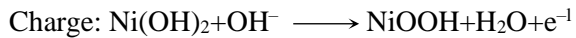
### Note 1: Reaction equations

The reaction equations are illustrated as follows:

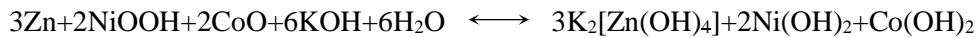
Anode:



Cathode:



Overall reaction:



## **Supporting References:**

1. L. Wang, K.-W. Huang, J. Chen and J. Zheng, *Sci. Adv.*, 2019, **5**, eaax4279.
2. Y. Zeng, Z. Lai, Y. Han, H. Zhang, S. Xie and X. Lu, *Adv. Mater.*, 2018, **30**, 1802396.
3. F. Wan, L. Zhang, X. Dai, X. Wang, Z. Niu and J. Chen, *Nat. Commun.*, 2018, **9**, 1656.
4. M. Yan, P. He, Y. Chen, S. Wang, Q. Wei, K. Zhao, X. Xu, Q. An, Y. Shuang, Y. Shao, K. T. Mueller, L. Mai, J. Liu and J. Yang, *Adv. Mater.*, 2018, **30**, 1703725.
5. J. Liu, C. Guan, C. Zhou, Z. Fan, Q. Ke, G. Zhang, C. Liu and J. Wang, *Adv. Mater.*, 2016, **28**, 8732-8739.
6. M. Gong, Y. Li, H. Zhang, B. Zhang, W. Zhou, J. Feng, H. Wang, Y. Liang, Z. Fan, J. Liu and H. Dai, *Energy Environ. Sci.*, 2014, **7**, 2025.
7. C. Xu, J. Liao, C. Yang, R. Wang, D. Wu, P. Zou, Z. Lin, B. Li, F. Kang and C. P. Wong, *Nano Energy*, 2016, **30**, 900-908.
8. H. Zhang, X. Zhang, H. Li, Y. Zhang, Y. Zeng, Y. Tong, P. Zhang and X. Lu, *Green Energy Environ.*, 2018, **3**, 56-62.
9. P. Zhang, Y. Li, G. Wang, F. Wang, S. Yang, F. Zhu, X. Zhuang, O. G. Schmidt and X. Feng, *Adv. Mater.*, 2019, **31**, 1806005.
10. Z. Tian, X. Tong, G. Sheng, Y. Shao, L. Yu, V. Tung, J. Sun, R. B. Kaner and Z. Liu, *Nat. Commun.*, 2019, **10**, 4913.
11. M. Qiu, P. Sun, G. Cui, Y. Tong and W. Mai, *ACS Nano*, 2019, **13**, 8246-8255.
12. J. Q. Xie, Y. Q. Ji, J. H. Kang, J. L. Sheng, D. S. Mao, X. Z. Fu, R. Sun and C. P. Wong, *Energy Environ. Sci.*, 2019, **12**, 194-205.
13. W. Yang, L. He, X. Tian, M. Yan, H. Yuan, X. Liao, J. Meng, Z. Hao and L. Mai, *Small*, 2017, **13**, 1700639.
14. J. Gao, C. Shao, S. Shao, F. Wan, C. Gao, Y. Zhao, L. Jiang and L. Qu, *Small*, 2018, **14**, 1801809.
15. C. J. Zhang, L. McKeon, M. P. Kremer, S. H. Park, O. Ronan, A. Seral-Ascaso, S. Barwick, C. O. Coileain, N. McEvoy, H. C. Nerl, B. Anasori, J. N. Coleman, Y. Gogotsi and V. Nicolosi, *Nat. Commun.*, 2019, **10**, 1795.
16. R. Guo, J. Chen, B. Yang, L. Liu, L. Su, B. Shen and X. Yan, *Adv. Funct. Mater.*, 2017, **27**, 1702394.
17. H. Wu, W. Zhang, S. Kandambeth, O. Shekhah, M. Eddaoudi and H. N. Alshareef, *Adv. Energy Mater.*, 2019, **9**, 1900482.
18. W. Li, H. C. Fu, Y. Zhao, J. H. He and S. Jin, *Chem*, 2018, **4**, 2644-2657.
19. N. Zhang, F. Huang, S. Zhao, X. Lv, Y. Zhou, S. Xiang, S. Xu, Y. Li, G. Chen, C. Tao, Y. Nie, J. Chen and X. Fan, *Matter*, 2020, **2**, 1-10.
20. X. Xu, S. Li, H. Zhang, Y. Shen, S. M. Zakeeruddin, M. Graetzel, Y. B. Cheng, and M. Wang, *ACS Nano*, 2015, **9**, 1782-1787.
21. A. Gurung, K. Chen, R. Khan, S. S. Abdulkarim, G. Varnekar, R. Pathak, R. Naderi and Q. Qiao, *Adv. Energy Mater.*, 2017, **7**, 1602105.
22. C. Li, S. Cong, Z. Tian, Y. Song, L. Yu, C. Lu, Y. Shao, J. Li, G. Zou, M. H. Rümmeli, S. Dou, J. Sun and Z. Liu, *Nano Energy*, 2019, **60**, 247-256.
23. J. Xu, Y. Chen and L. Dai, *Nat. Commun.*, 2015, **6**, 8103.
24. J. Liang, G. Zhu, C. Wang, P. Zhao, Y. Wang, Y. Hu, L. Ma, Z. Tie, J. Liu and Z. Jin, *Nano Energy*, 2018, **52**, 239-245.
25. B. P. Lechêne, M. Cowell, A. Pierre, J. W. Evans, P. K. Wright and A. C. Arias, *Nano Energy*, 2016, **26**, 631-640.